JOURNAL OF MATERIALS SCIENCE 29 (1994) 2813–2820

X-ray diffraction study of mechanically alloyed amorphous-crystalline titanium silicides

N. ZOTOV
Institute of Applied Mineralogy, Bulgarian Academy of Sciences, Rakovski str. 92, Sofia 1000, Bulgaria

D. PARLAPANSKI
Department of Mineral Processing, University of Mining and Geology, Sofia 1156, Bulgaria

The structure of mechanically alloyed (MA) Ti–Si powders has been investigated by means of X-ray diffraction radial distribution functions analysis and computer-generated quasi-crystalline models. It was established that the investigated samples with compositions $Ti_{33}Si_{67}$ and $Ti_{42}Si_{58}$ consist of an amorphous matrix, with chemical short-range order (SRO) similar to that of the TiSi phase, in which crystallites of the Ti_5Si_3 and Ti_5Si_4 phases are embedded. For the composition $Ti_{44}Si_{56}$, the SRO resembles the structural arrangement in the Ti_5Si_3 phase. An attempt has been made to explain these results using the formation enthalpies of the amorphous and the crystalline phases formed in earlier stages of MA. The Ti_5Si_4 and Ti_5Si_3 phases have a much lower formation enthalpy than the other Ti–Si phases. That is why the amount of mechanical energy imparted during MA is not sufficient completely to drive the amorphization in these two phases.

1. Introduction

The preparation of amorphous alloys by mechanical alloying (MA) is attracting growing attention, from both the scientific and technological points of view. It represents a high-energy ball-milling technique and has been applied initially for the production of oxide dispersion-strengthened alloys, corrosion-resistive alloys and alloys of otherwise immiscible components [1, 2].

More recently it has been shown that this process could also lead to amorphous metallic alloy formation [3, 4]. In the comprehensive studies of Schwarz *et al.* [5] on the Ti–Ni system and Schultz and Hellstern [6, 7] on the Zr–TM systems, where TM is a last transition metal in the fourth period of Mendeleev's table, it was found that this process proceeds via the formation of composite powder particles consisting of alternate layers of the starting constituents. Amorphization was explained by a diffusion-controlled solid-state chemical reaction initiated at the interfaces of these elemental layers. Two prerequisites should be fulfilled for that purpose:

(i) a large negative enthalpy of mixing of the alloying elements;

(ii) one of the alloying elements should be a fast diffuser in the other.

The first prerequisite ensures the thermodynamic driving force of the reaction, while the second one is crucial for the amorphization.

However, this type of amorphization has been reported recently for systems possessing a positive enthalpy of mixing such as Cu–Ta [8], Cu–V [9] and Cu–Cr [10], as well as for the V–Zr system, where there is no fast diffusion [11].

Another kind of amorphization by MA is observed in systems in which crystalline intermetallic compounds are formed initially, which in turn transform to the amorphous state on continued milling. This transformation can be attributed to the accumulation of point defects which raise the free energy of the crystalline phases above that of their amorphous counterparts [12].

The Ti–Si system is interesting because of its potential technological applications. Crystalline titanium silicides are known as corrosion-resistive compounds [13]. $TiSi_2$, with C54 type structure, is an excellent candidate for application in integrated circuit interconnection schemes [14]. Silicon- and titanium-containing compounds were widely used in catalysis [15]. Obviously it is also interesting to obtain and investigate amorphous titanium silicides.

Polk *et al.* [16] have reported the formation of amorphous $Ti_{80}Si_{20}$, by rapid quenching from the liquid state. By this method amorphous alloys can be obtained in a narrow range located in the vicinity of deep eutectic lines. More recently, amorphous Ti–Si thin film alloys, produced in a wider concentration range by annealing of multilayers [17] or by co-sputtering [18], have been investigated.

As it will be shown below, the Ti–Si system has a strong negative enthalpy of formation in the amorphous state. On the other hand, a high diffusion constant with a value of 3.31×10^{-15} $cm^2 s^{-1}$ has been derived [17] for the diffusion of silicon in titanium in thin-film multilayers upon 400 °C annealing. These facts suggest that amorphization by MA can be expected for this system.

MA in the Ti–Si system was reported for the first

0022–2461 © *1994 Chapman & Hall*

time by Veltl *et al.* [19], and more recently by Parlapanski *et al.* [20], and Calka *et al.* [21]. A different evolution of the structure of the Ti–Si powders during milling was observed by Veltl *et al.* [19] and Parlapanski *et al.* [20]. Parlapanski *et al.* [20] reported the formation of crystalline titanium silicides after 4 h milling, which are later transformed into an amorphous state, while Veltl *et al.* [19] observed a continuous decrease of the intensities of the Bragg peaks of the elemental powders until a broad amorphous maximum appeared. The differences between these two studies can be attributed to the different ball-milling equipment used. Veltl *et al.* [19] used a planetary ball mill, while Parlapanski *et al.* [20] used a vibro mill and a much larger ball-to-powder weight ratio. In the study of Calka *et al.* [21], the process was conducted in a planar cell, with a controlled ball movement. They investigated two different compositions: Ti_5Si_3 and $TiSi_2$. Complete amorphization after 180 h milling was observed in the first case, while in the second case, amorphization did not occur even after 500 h milling.

One essential feature of the MA in the Ti–Si system reported by both Veltl *et al.* [19] and Parlapanski *et al.* [20], is that after the amorphous structure has been formed, further milling causes some changes in the X-ray diffraction patterns. They can be interpreted as a partial crystallization [19], or a decomposition to different amorphous phases, some of them exhibiting an increased degree of ordering [20]. However, after additional milling up to 45 h [19] and 36 h [20], complete amorphization again takes place.

Because there have been no systematic structural investigations of MA Ti–Si amorphous alloys, we have carried out X-ray radial distribution function analysis of Ti–Si alloys, obtained by MA from pure elemental powders. The results are reported here.

2. Experimental procedure

2.1. Sample preparation

The blends of silicon powder with particle size less than 320 μm, and 1–2 mm coarse titanium flakes, were milled in a vibro-mill with a hardened steel vial and WC–Co doped milling tools under an argon atmosphere. The vial was charged with titanium and silicon powders in appropriate weight proportions, filled with argon via an argon flux, and sealed with silicate plaster. The weight ratio of the milling tools to the powder was 70:1, due to the high density of the WC. The vial vibrated during the milling with an amplitude of 2.5 cm. The milling process was in intervals of 12 h milling and 12 h rest. In order to reduce the adherence of the powder to the surfaces of the vial and balls, the vial was rotated at 3 h intervals. No outer cooling was supplied. Only powders free from sticking and agglomeration were used for structural characterization. In an effort to obtain more homogeneous samples, suitable for X-ray diffraction measurement, we extended the milling up to 60 h only for samples $Ti_{50}Si_{50}$, $Ti_{55}Si_{55}$ and $Ti_{60}Si_{40}$, reported elsewhere [20], because beyond this region strong impurities of WC have been observed [20].

The compositions of the final MA products were analysed using a Philips 513 SEM with EDAX X-ray dispersive analyser (Table I). The samples $Ti_{33}Si_{67}$, $Ti_{42}Si_{58}$ and $Ti_{44}Si_{56}$ are denoted in the text TS1, TS2 and TS3, respectively.

2.2. X-ray data collection

The X-ray diffraction experiments were performed using zirconium-filtered MoK_α radiation on a DRON 3M powder diffractometer with 1°30′ Soller slits in the incident and diffracted beams, a divergence slit of 1° and a receiving slit of 0.15°. A scintillation counter and a pulse-height discriminator were used. The powdered samples were pressed in a plexiglass sample holder. All measurements were made in reflection geometry, in the angular range $10° \leqslant 2\theta \leqslant 130°$ corresponding to a Q range from 0.17–16 A^{-1}, where $Q = 4\pi\sin\theta/\lambda$ is the scattering vector, 2θ is the scattering angle and λ is the length of the radiation used. The spectrum was scanned with a constant step 0.25° 2θ for $10° < 2\theta < 35°$ and 0.5° 2θ for $2\theta > 35°$. The intensities were measured five times using a fixed time per step (10 s) and the results were averaged.

2.3. X-ray data reduction and calculation of the radial distribution functions

The raw experimental data were corrected for counter deadtime, background and substrate scattering, polarization and absorption in the sample in the usual way [22]. The corrected intensity is converted into electronic units, by both the Krogh–Moe [23] and the high-angle methods.

The coherently scattered intensity per atom, $I_{coh}(Q)$, is obtained from

$$I_{coh}(Q) = \beta I_{cor}(Q) - [A(Q)_{incoh} I_{incoh}(Q) + A(Q)_{SA} I_{SA}(Q)]/A(Q)_{coh} \quad (1)$$

where $A(Q)$ is the absorption correction. The subscripts coh, incoh, and SA denote coherent, incoherent and small-angle scattering, respectively. The incoherent scattering was calculated from published regression coefficients [24], taking into account the Breit–Dirac recoil factor.

TABLE I Composition of mechanically alloyed Ti–Si powders

Sample	Element	Starting blends		Final alloys
		(wt %)	(at %)	Measured (at %)
TS1	Ti	50	37	33.37
	Si	50	63	66.00
	Fe	–	–	0.23
	W	–	–	–
TS2	Ti	55	42	41.55
	Si	45	58	57.87
	Fe	–	–	0.41
	W	–	–	0.17
TS3	Ti	60	47	44.38
	Si	40	53	55.38
	Fe	–	–	0.24
	W	–	–	–

According to the Faber–Ziman definition, the total structure factor, $S(Q)$ is related to I_{coh} by

$$S(Q) = [I_{coh}(Q) - (\langle f^2 \rangle - \langle f \rangle^2)]/\langle f \rangle^2 \quad (2)$$

where $\langle f \rangle$ and $\langle f^2 \rangle$ are the mean and the mean square scattering factors which were calculated from analytical expressions [25] and corrected for anomalous dispersion [26].

The reduced radial distribution function, $G(r)$, was calculated according to

$$G(r) = 2/\pi \int_0^{Q_{max}} Q[S(Q) - 1]M(Q)\sin(Qr)\,dr \quad (3)$$

where $M(Q)$ is a modification function of the form $M(Q) = \sin(\alpha Q)/(\alpha Q)$ [27], where the values of α were chosen according to the condition $M(Q_{max}) = 0.01$.

Finally, the $G(r)$ functions were corrected by the method proposed by Kaplow *et al.* [28]. The computer program used was written by one of the authors [29].

3. Results

3.1. X-ray diffraction patterns

Fig. 1 shows the X-ray diffraction patterns of the investigated samples in the angular range from 10° 2θ to 35° 2θ. A strong first diffraction maximum at about 17° 2θ, a second maximum at about 22° 2θ and several very weak, broad and overlapping peaks up to 35° 2θ, are observed. Closer examination shows that the first diffraction maximum of samples TS2 and TS3 is split into more than one peak.

Several points can be inferred from these X-ray diffraction patterns.

(i) New phases have been formed after 60 h milling time in comparison with the X-ray diffraction patterns of the starting blends (Fig. 1).

(ii) Evidently, there is no complete amorphization, in spite of the prolonged milling time. The peaks observed, can be explained by the formation of stable intermetallic alloys. According to the Ti–Si phase diagram, given by Barabash and Koval [30], the following Ti–Si phases can be present at room temperature: TiSi, Ti_3Si, Ti_5Si_3, Ti_5Si_4 and $TiSi_2$. The TiSi phase exists in three modifications – an orthorhombic one with a space group (SG) $Cmmm$ [31], a second one with FeB-type structure and a SG $Pnma$ [32–34], and a third one with a SG $Pmm2$ [35]. Only one phase, Ti_3Si, exists with a Ti_3P-type structure and a SG $P4_12n$ [36, 37]. The Ti_5Si_3 phase also exists only in one modification with a Mn_5Si_3-type structure and a SG $P6_3/mcm$ [32, 37, 38]. The Ti_5Si_4 phase exists in two modifications – Ti_5Si_4-type modification with a SG $Pnma$ [39] and a second modification with Zr_5Si_4-type structure and a SG $P4_12_12$ [37, 40]. The $TiSi_2$ phase also exists in two modifications – the first one with a $TiSi_2$-type structure and a SG $Fddd$ [37, 41, 42], and a second one with a $ZrSi_2$-type structure and a SG $Cmcm$ [33, 43].

A comparison of the XRD patterns of the titanium silicides mentioned above and the experimentally observed residual diffraction peaks, was made. The residual peaks in the TS1 sample best resemble the Ti_5Si_3 phase, while those in the TS2 and the TS3 samples have been identified as belonging to the Ti_5Si_3 and Ti_5Si_4 phases. Traces of $TiSi_2$ are also possible.

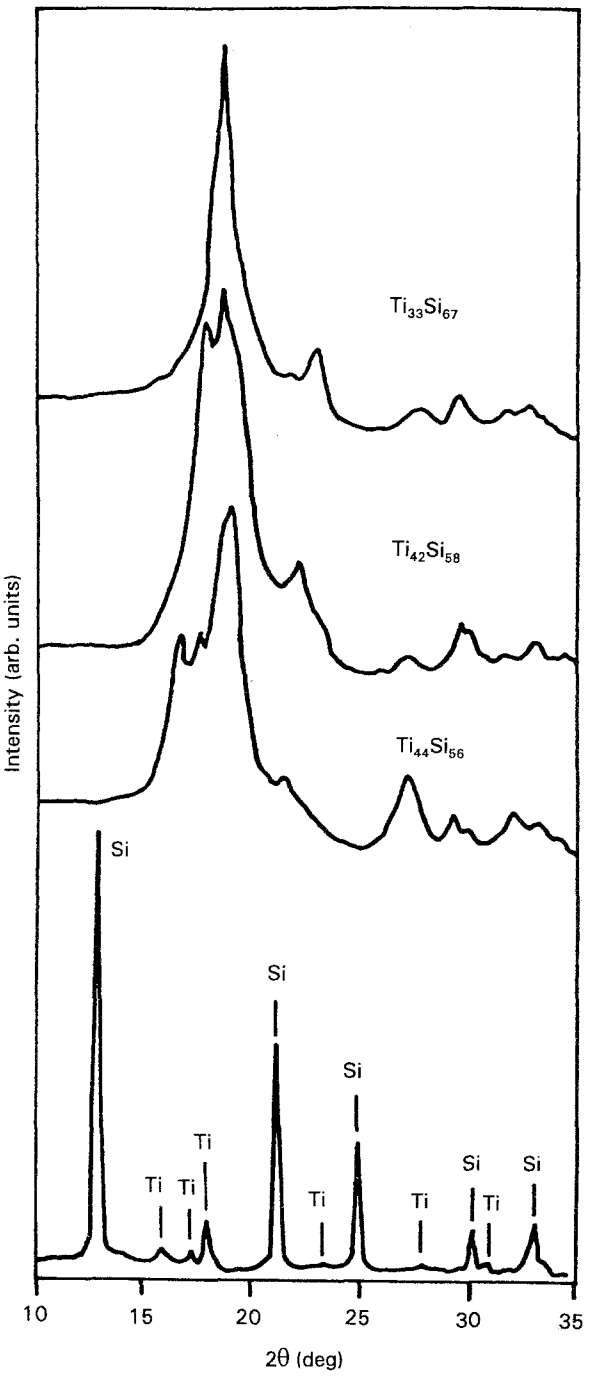

Figure 1 X-ray diffraction patterns of Ti–Si MA samples $Ti_{33}Si_{67}$, $Ti_{42}Si_{58}$, $Ti_{44}Si_{56}$ and a starting blend with weight ratio Ti:Si = 1:1 (MoK_α radiation).

(iii) The phases obtained by MA, therefore, may be either microcrystalline intermetallic compounds, or a mixture of amorphous and intermetallic phases.

In order to examine further these structural possibilities, we have plotted in Fig. 2 the coherently scattered intensities in absolute units in the whole angular range $0 \leqslant Q \leqslant 16\ A^{-1}$. The coherent intensity curves, $I_{coh}(Q)$, consist of a part slowly oscillating around $\langle f^2 \rangle$ on which more or less narrow peaks with decreasing intensities are superimposed. Evidently, the general behaviour of the curves is characteristic for an amorphous phase. However, the number and the full

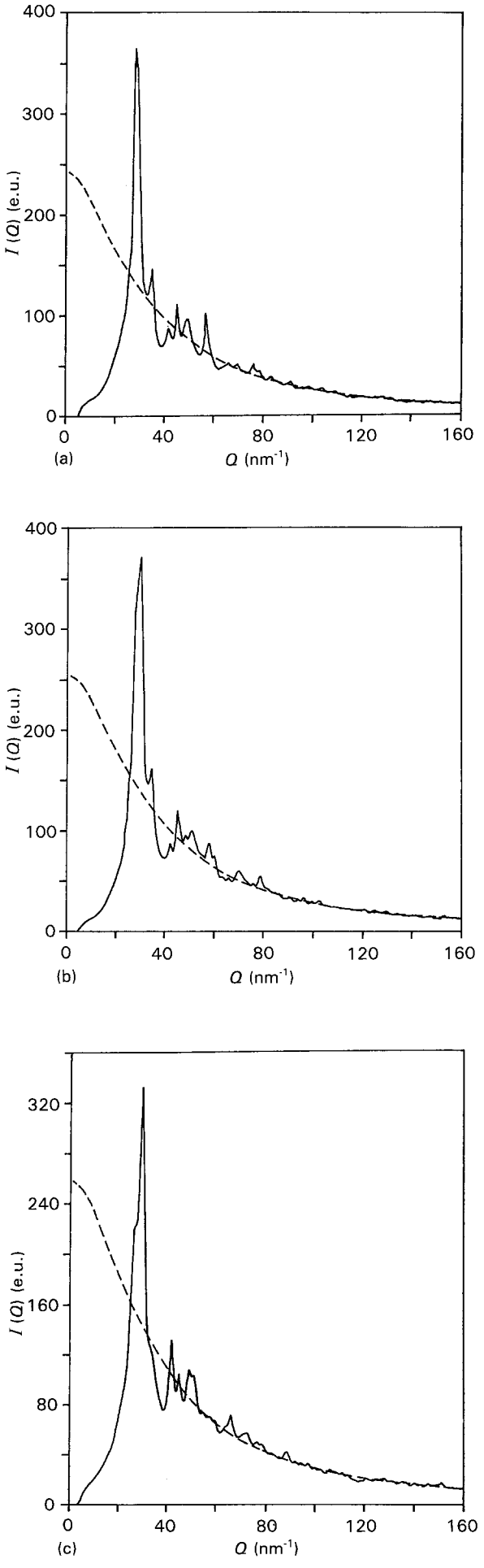

Figure 2 Normalized coherently scattered intensity curves: (a) $Ti_{33}Si_{67}$, (b) $Ti_{42}Si_{58}$, (c) $Ti_{44}Si_{56}$. (– – –) Independent scattering $\langle f^2 \rangle$.

width at half maximum (FWHM) of the peaks suggest a larger crystalline order than could be expected for a purely amorphous state. Therefore, it may be assumed that the MA powders investigated represent an amorphous matrix in which are embedded microcrystals of certain intermetallic phases. However, at this point it is difficult to determine the exact volume fraction of the microcrystalline phases.

3.2. Radial distribution functions

The reduced radial distribution functions, $G(r)$, are given in Fig. 3. The insets show the corresponding total pair distribution function TPF(r)

$$\mathrm{TPF}(r) = 1 + G(r)/2\pi^2\rho_0 r \qquad (4)$$

where ρ_0 is the mean atomic number density.

The corresponding total radial distribution functions, $\mathrm{RDF}(r) = 4\pi r^2\rho_0 + rG(r)$, are given in Fig. 4. The positions of the first several peaks of the $G(r)$

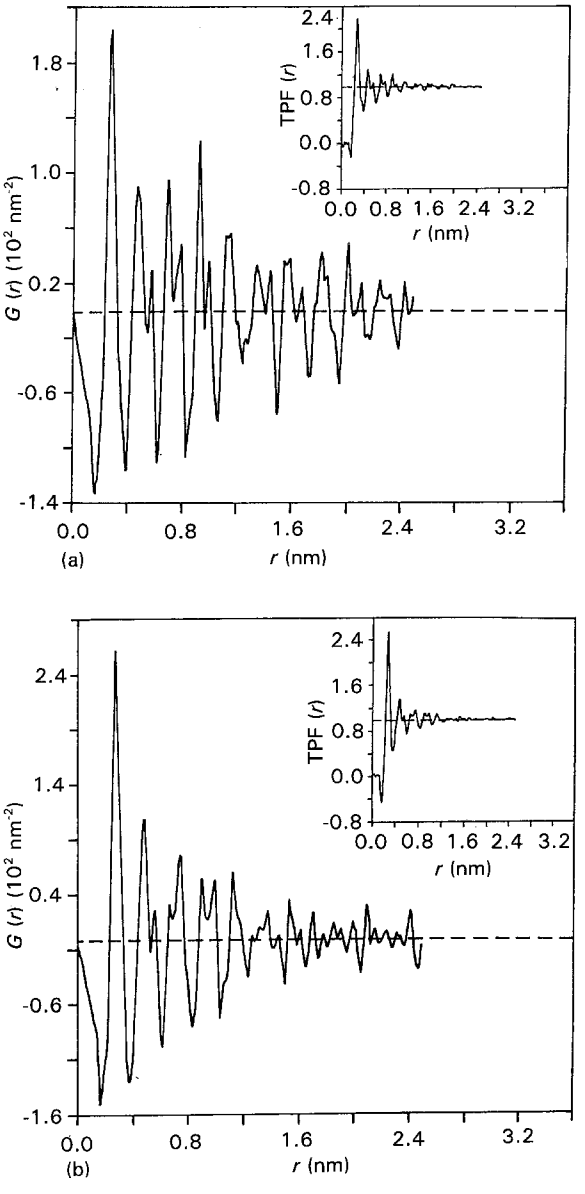

Figure 3 Reduced radial distribution functions $G(r)$ and the corresponding total pair correlation functions TPF(r): (a) $Ti_{33}Si_{67}$, (b) $Ti_{42}Si_{58}$, (c) $Ti_{44}Si_{56}$.

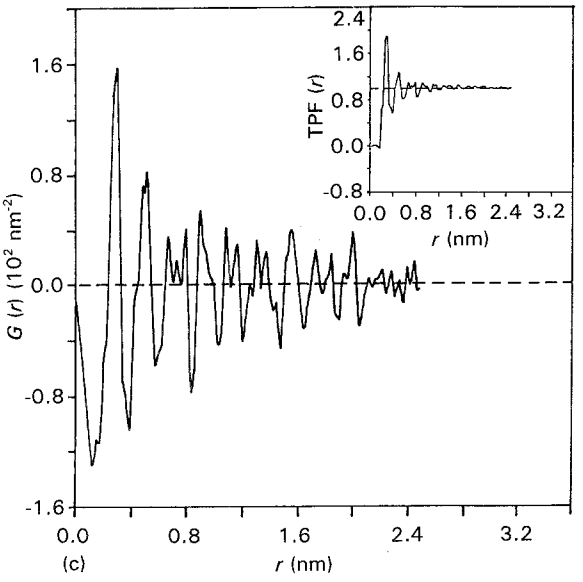

Figure 3 (continued)

functions along with the first coordination numbers, N_1, and the corresponding correlation lengths, L_c, are given in Table II. The coordination numbers, N_1, are obtained by integrating the first maximum of the RDF(r) to the position of the first minimum in RDF(r). The correlation lengths L_c were deduced from the corresponding TPF(r) functions using Masumoto *et al.*'s criterion [44] according to which, for $r \geqslant L_c$, the TPF(r) function should fulfill the condition $1 - \varepsilon \leqslant \mathrm{TPF}(r) \leqslant 1 + \varepsilon$, with $\varepsilon = 0.1$.

The splitting of the second peak of the $G(r)$ functions in samples TS1 and TS2 and the positions of the two shoulders, scaled to the first peak position – r_1/r_2 and r_1/r_{2a} (see Table II) are characteristic for transition metal–metalloid alloys [45]. The number of the first nearest neighbours, N_1, is similar to that of amorphous $Pd_{80}Si_{20}$ alloy, prepared by melt spinning [45]. The general form of the TPF(r) function also confirms the amorphous nature of the investigated MA samples. The comparison of the form of the RDFs (Fig. 4) and the interatomic distances given in Table II shows that samples TS1 and TS2 have, in contrast with sample TS3, similar local structure.

However, the observed high correlation lengths, L_c, and degree of crystallinity $\xi = L_c/r_1$ [45] indicate that either there are microcrystals embedded in the amorphous matrix, as previously suggested, or the amorphous matrix exhibits larger intermediate range order.

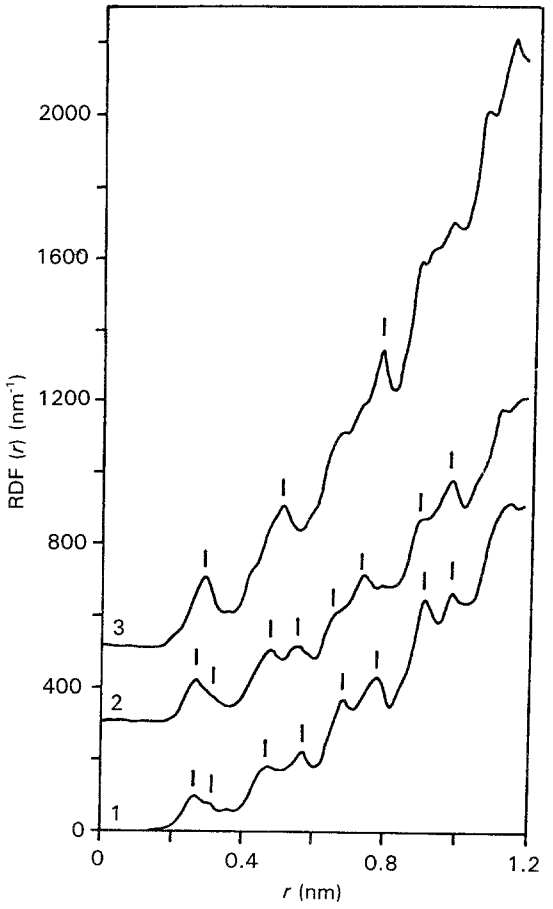

Figure 4 Total radial distribution functions RDF(r), 1, $Ti_{33}Si_{67}$; 2, $Ti_{42}Si_{58}$; 3, $Ti_{44}Si_{56}$.

3.3. Quasi-crystalline radial distribution functions

In order to study further the structural state of the MA samples investigated, we have calculated total RDF(r) functions from quasi-crystalline models (QCM), based on the structure of different Ti–Si intermetallic compounds. The method of Taylor [46] has been used. The quasi-crystalline radial distribution functions (QCM RDF) have been calculated as a Fourier transformation of the corresponding quasi-crystalline model intensity functions, defined by

$$I_{\mathrm{QCM}}(Q) = \sum_i \sum_j f_i(Q) f_j(Q) \exp(-b_{ij}Q^2) \sin Qr_{ij}/Qr_{ij} + I_{\mathrm{SA}}(Q) \quad (5)$$

with

$$b_{ij} = (B_i + B_j)/8\pi^2 + (r_{ij}/kr_c)^2 \quad (6)$$

TABLE II Selected results from the XRD RDF analysis

Sample	N_1	L_c (nm)	r_1 (nm)		r_j^b/r_1						
				ξ^a	$j=2$	$2a$	3	4	5	6	7
TS1	11.5 ± 1.0	2.2 ± 0.1	0.275 ± 0.002	8.0	1.73	2.07	2.52	2.82	3.34	3.60	4.13
TS2	10.0 ± 0.5	1.8 ± 0.1	0.275 ± 0.002	6.5	1.73	2.00	2.44	2.72	3.27	3.60	4.10
TS3	10.2 ± 0.5	2.1 ± 0.1	0.286 ± 0.002	7.7	1.73	–	2.36	2.62	2.80	3.17	3.79

[a] $\xi = L_c/r_1$ [45]
[b] j is the consecutive number of the peaks in the corresponding $G(r)$ functions.

and

$$I_{SA}(Q) = \sum_i \sum_j f_i(Q) f_j(Q)\, 4\pi\rho_0 [Qr_c \cos(Qr_c) - \sin(Qr_c)]/Q^3 \quad (7)$$

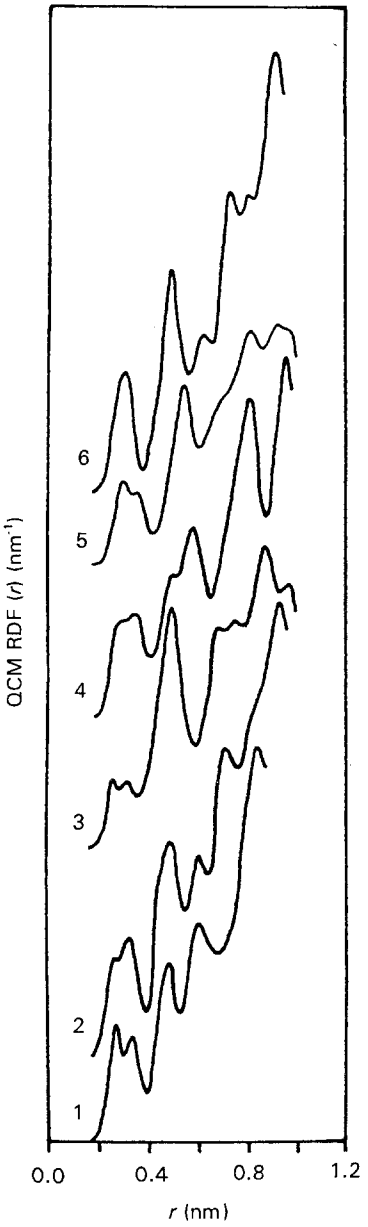

Figure 5 Quasi-crystalline total radial distribution functions QCM RDF(*r*): 1, TiSi (SG P*nma*); 2, TiSi (SG P*mm*2; 3, $TiSi_2$ (SG F*ddd*); 4, $TiSi_2$ (SG C*mcm*); 5, Ti_5Si_4 (SG P4 2 2); 6, Ti_5Si_3 (SG $P6_3/mcm$)

where B_i and B_j are the isotropic temperature factors of the corresponding atoms, k is an adjustable constant and r_c is the radius of the cluster used. The value of k has been taken equal to 5. The calculated QCM RDF functions are given in Fig. 5 and the first nearest-neighbour distances and the corresponding coordination numbers in some Ti–Si intermetallic compounds, are shown in Table III.

A comparison of the QCM RDF(*r*) and the experimental RDF indicates that the position of the RDF(*r*) peaks below 0.6 nm in samples TS1 and TS2 resembles best the short-range order in the TiSi phase with FeB-type structure. On the contrary, the experimental radial distribution function of sample TS3 is very close to the QCM RDF of the Ti_5Si_3 phase.

A systematic pair correlations assignment of the peaks of the experimental RDF(*r*) will be published in the future. However, even now the interatomic distances, given in Table III, show that the first peak of RDF(*r*) is composed simultaneously of nearest-neighbour atom pairs Ti–Ti, Ti–Si and Si–Si.

4. Discussion

The main question remaining open from the technological point of view is why milling up to 60 h cannot produce purely amorphous state for the particular system investigated. The answer could be sought in the kinetics of phase formation in earlier milling stages. The peaks observed in the XRD pattern of the $Ti_{42}Si_{58}$ sample after 4 h milling time [20] can be identified as belonging to the TiSi, $TiSi_2$, Ti_5Si_3 and the Ti_5Si_4 phases. This suggests that solid-state chemical reactions have occurred and that they lead to the formation of crystalline phases existing in the phase diagram. Any defect in the crystal lattice produced by further milling would raise their free energy. If the free energy of the distorted crystalline phase becomes higher than the free energy expected for its amorphous counterpart, the phase should make a transition to the amorphous state. This amorphization mechanism has been proposed and discussed by Schwarz and Koch [12]. The X-ray diffraction results presented here indicate that such a transition to the amorphous state is obviously not accomplished.

To understand this event, the formation enthalpies of the different phases produced by MA should be

TABLE III Interatomic distances and coordination numbers (CN) found in intermetallic Ti–Si compounds

Phase	Space group	Reference	Interatomic distances					
			Ti–Si		Si–Si		Ti–Ti	
			R (nm)	CN	*R* (nm)	CN	*R* (nm)	CN
TiSi	P*nma*	[32–34]	0.260–0.271	7	0.221	2	0.322–0.349	8
TiSi	P*mm*2	[35]	0.230–0.281	6	0.275–0.291	–	0.307–0.361	8
$TiSi_2$	F*ddd*	[37,41] [42]	0.254	4	0.254–0.275	5	0.319	4
$TiSi_2$	C*mcm*	[33,42]	0.275–0.337	10	0.255	2–4	0.360–0.362	4
Ti_5Si_4	$P4_12_12$	[37,40]	0.260–0.307	6	0.247	–	0.302–0.382	7–9
Ti_5Si_3	$P6_3/mcm$	[32,37] [38]	0.254–0.280	5–6	0.305	–	0.310–0.317	6–7

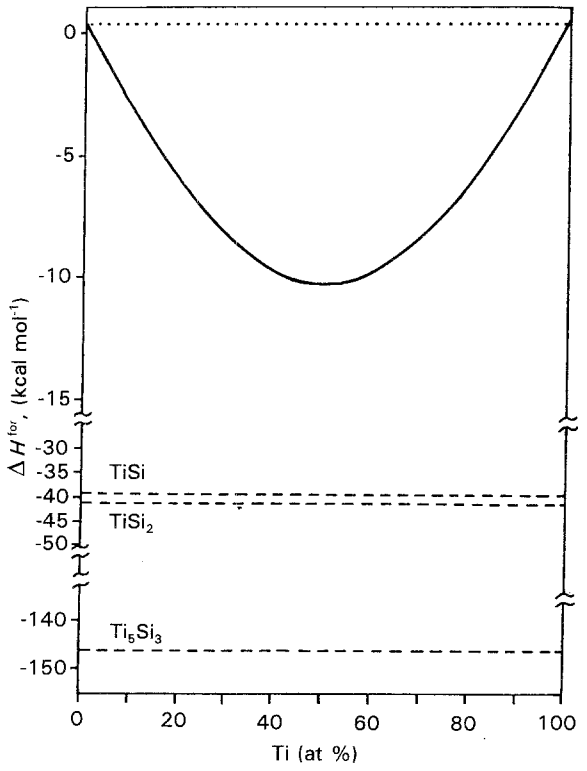

Figure 6 Formation enthalpy diagram: (——) amorphous Ti–Si alloy; (– – –) crystalline Ti–Si intermetallic compounds; (···) mechanical mixture of elemental titanium and silicon.

taken into account. Fig. 6 is a formation enthalpy diagram of the Ti–Si system. The dashed lines indicate the formation enthalpy levels of the stable crystalline titanium silicides. The enthalpies of formation of the phases TiSi, $TiSi_2$ and Ti_5Si_3 have been taken from the literature [47]. Taking into account the similarity in the melting points of Ti_5Si_4 and Ti_5Si_3 [13, p. 50] it can be expected that the Ti_5Si_4 phase would have ΔH^{for} close to that of the Ti_5Si_3 phase. The solid line represents the formation enthalpy of the amorphous phase as a function of the composition, calculated following the method proposed by Loeff *et al.* [48]. The dotted line gives the formation enthalpy of a mixture of elemental titanium and silicon. It is seen that the phase Ti_5Si_3 has a strong negative enthalpy of formation of about -145 kcal mol^{-1}, while the other two phases TiSi and $TiSi_2$ have ΔH^{for} of about -40 kcal mol^{-1}.

Let us now consider the behaviour of these phases in the light of this formation enthalpy diagram. It can be seen that an increase in the free energy of the TiSi and $TiSi_2$ phases, associated with an increase in the ΔH^{for} term, of about 30–35 kcal mol^{-1} would be sufficient for triggering the transition to the amorphous state, but such an increase in ΔH^{for} would be insufficient for the Ti_5Si_3 and Ti_5Si_4 phases: an increase of more than 135 kcal mol^{-1} would be needed for their amorphization. However, such a large increase of ΔH^{for} during MA under our experimental conditions is highly inconceivable, because an increase in ΔH^{for} of more than 40–50 kcal mol^{-1} would result in a decomposition of the TiSi and $TiSi_2$ phases to elemental titanium and silicon. Such a decomposition has been reported and explained in the same way for binary lanthanum-based alloys [49], but it was not observed in our XRD study. Thus, it can be concluded that MA in our milling equipment raises the free energy of the titanium silicides, with no more than a 30–40 kcal mol^{-1} increase in the enthalpy term. Therefore, complete amorphization should not be expected for the Ti_5Si_3 and Ti_5Si_4 phases. This explains quite well the presence of residual XRD peaks of these phases. Evidently, the change in the XRD patterns after 12 h milling, observed by Parlapanski *et al.* [20] can be connected with amorphization of the TiSi and $TiSi_2$ phases, which have considerably higher ΔH^{for}, and only a broadening of the peaks of the Ti_5Si_3 and Ti_5Si_4. This mechanism of amorphization during MA suggests that the local order of the amorphous matrix must resemble the chemical short-range order of the TiSi and $TiSi_2$ phases which is observed, at least for the TS1 and TS2 samples, when comparing the QCM RDF(r) and the experimental RDF(r). The fact that the short-range order in sample TS3 resembles that of Ti_5Si_3 requires additional investigation. At this point it is worth rementioning the study of Calka *et al.* [21], who were able to obtain amorphous Ti_5Si_3 after 180 h milling. Obviously their milling equipment was able to impart the increase in ΔH^{for} required to produce amorphization of this phase.

5. Conclusions

Ti–Si alloys were prepared by mechanical alloying (MA) of elemental titanium and silicon powders in a vibro mill, with 60 h milling time. X-ray diffraction RDF analysis of the structure of $Ti_{33}Si_{67}$, $Ti_{42}Si_{58}$ and $Ti_{44}Si_{56}$-alloys has been carried out. The following results were established.

1. The X-ray diffraction patterns, and the corresponding RDF(r) indicate the presence of an amorphous structure, with some regions exhibiting larger local ordering, which may be attributed to the existence of Ti_5Si_3 and/or Ti_5Si_4 crystallites.

2. The partially crystalline nature of the investigated samples is confirmed by the large correlation lengths ($L_c \approx 2$ nm) and the high degree of crystallinity ($\xi \approx 7$) observed.

3. The short-range order (SRO) in the $Ti_{33}Si_{66}$ and $Ti_{42}Si_{58}$ samples resembles that in the TiSi intermetallic compound with FeB-type structure, while the SRO in the $Ti_{44}Si_{56}$ sample is similar to that of the Ti_5Si_3 phase.

4. This amorphous–crystalline nature can be explained by the vastly different formation enthalpies of the crystalline TiSi, $TiSi_2$, Ti_5Si_3 and Ti_5Si_4 phases, which are formed in earlier stages of MA. It may be suggested that during the 60 h MA of the Ti–Si system under our experimental conditions, amorphization occurs predominantly of the TiSi and $TiSi_2$ phases, and only disordering is seen of the Ti_5Si_3 and Ti_5Si_4 phases, which have strongly negative enthalpies of formation.

References

1. J. S. BENJAMIN, *Sci. Am.* **234** (5) (1976) 40.
2. R. SUNDARESAN and F. H. FROES, *J. Metals* **39** (1987) 22.

3. R. L. WHITE, PhD thesis, Stanford University (1979).
4. C. C. KOCH, O. B. CARIN, C. G. McCAMEY and J. O. SCARBROUGH, *Appl. Phys. Lett.* **43** (1983) 1017.
5. R. B. SCHWARZ, R. R. PETRICH and C. K. SAW, *J. Non-Cryst. Solids* **76** (1985) 281.
6. L. SCHULTZ and E. HELLSTERN, in "Materials Research Society Symposium Proceedings", Vol. 80 (Materials Research Society, Pittsburgh, PA, 1987).
7. E. HELLSTERN and L. SCHULTZ, *J. Appl. Phys.* **63** (1988) 1408.
8. T. FUKUNAGA, K. NAKAMURA, K. SUZUKI and U. MIZUTANI, *J. Non-Crystalline Solids* **117/118** (1990) 700.
9. T. FUKUNAGA, M. MORI, K. INOU and U. MIZUTANI, *Mater. Sci. Eng. A*, in press.
10. Y. OGINO, S. MURAYAMA and T. YAMASAKI, *J. Less-Common Metals* **168** (1991) 221.
11. A. W. WEEBER and H. BAKKER, *Z. Chem. Phys. N. F.* **157** (1988) 221.
12. R. B. SCHWARZ and C. C. KOCH, *Appl. Phys. Lett.* **49** (1986) 146.
13. G. V. SAMSONOV, L. A. DVORINA and B. M. RUD, "Silicides" (Metallurgia, Moscow, 1979) p. 73 (in Russian).
14. S. P. MURARKA, "Silicides for VSLI application" (Academic Press, New York, 1983).
15. V. A. REUTER (ed.), "Catalitic Properties of the Substances. A Handbook", Vol. II, Book I (Naukova Dumka, Kiev, 1975) (in Russian).
16. D. E. POLK, A. CALKA and B. C. GIESSEN, *Acta Metall.* **26** (1978) 223.
17. K. HOLLOWAY and R. SINCLAIR, *J. Less-Common Metals* **140** (1988) 139.
18. I. J. M. M. RAAIJMAKERS, A. H. van OMEN and A. H. READER, *J. Appl. Phys.* **65** (1989) 3896.
19. G. VELTL, B. SCHOLZ and H. D. KUNZE, in "Proceedings of the DGM Conference on New Materials by Mechanical Alloying Techniques", edited by E. Arzt and L. Schultz (Deutsche Gesellschaft fur Metallkunde e.v., 1989) p. 79.
20. D. PARLAPANSKI, S. DENEV, S. RUSEVA and E. GATEV, *J. Less-Common Metals* **171** (1991) 231.
21. A. CALKA, A. P. RADLINSKI, R. A. SHANKS and A. P. POGANY, *J. Mater. Sci. Lett.* **10** (1991) 43.
22. A. C. WRIGHT, *Adv. Struct. Devel. Diffr. Methods* **5** (1974) 1.
23. J. KROGH-MOE, *Acta Crystallogr.* **9** (1956) 951.
24. H. H. M. BALYNZI. *ibid. A* **31** (1975) 600.
25. D. T. CROMER and J. B. MAN, *ibid. A* **24** (1968) 321.
26. D. T. CROMER, *ibid.* **18** (1965) 17.
27. E. LORCH. *J. Phys. C* **2** (1969) 229.
28. R. KAPLOW, B. L. AVERBACH and S. L. STRONG, *J. Phys. Chem. Solids* **25** (1964) 1195.
29. N. ZOTOV, in "Proceedings of 2nd National Conference on X-ray Diffraction Methods". Primorsko, May 1984 (Sofia University Press, Sofia. 1985) pp. 134–9.
30. O. M. BARABASH and N. KOVAL, "Crystal Structure of Metal and Alloys" (Naukova Dumka, Kiev, 1986) p. 553 (in Russian).
31. J. J. NICKL and K. SCHWEITZER, *Z. Metallkde* **61** (1970) 55.
32. M. HANSEN, H. D. KESSLER and D. J. McPHERSON, *Trans. Am. Soc. Metall.* **44** (1952) 518.
33. C. BRUKL, H. NOVOTNY, O. SCHOB and F. BENESOVSKI, *Mh. Chem.* **92** (1961) 781.
34. K. NOVOTNY, B. LUX and H. KUDIELKA, *ibid.* **87** (1956) 447.
35. N. AGEEV and V. SAMSONOV, *Dokl. Acad. Nauk SSSR* **112** (1957) 853.
36. W. RO TEUTSCHER and K. SCHUBERT, *Z. Metallkde* **56** (1965) 813.
37. V. N. SVECHNIKOV, U. A. KOCHERZINSKII, L. M. UPKO, O. G. KULIK and E. A. SHISHKIN, *Dokl. Acad. Nauk SSSR* **193** (1970) 393.
38. P. PIETROKOWSKI and P. DUWEZ, *J. Metals* **3** (1951) 772.
39. J. J. NICKL and H. SPRENGER, *Z. Metallkde* **60** (1969) 136.
40. H. SPRENGER and J. J. NICKL, *Naturwiss.* **54** (1967) 645.
41. F. LAVES and H. J. WALLBAUM, *Z. Kristallogr. A* **101** (1939) 78.
42. H. NOWOTNY, H. SCHROTH, R. KIEFFER and F. BENESOVSKY, *Mh. Chem.* **84** (1953) 582.
43. G. COTTER, J. A. KOHN and R. A. POTTER, *J. Am. Ceram. Soc.* **39** (1956) 1.
44. T. MASUMOTO, Y. WASEDA, H. KIMURA and A. INOUE, *Sci. Rep. RITU A* **26** (1976) 21.
45. K. SUDZUKI, H. FUJIMORI and K. HASIMOTO, "Amorphous Metals", Translated from Japanese (Metallurgia, Moscow, 1987) (in Russian).
46. M. TAYLOR, *J. Appl. Crystallogr.* **12** (1979) 442.
47. U. M. GOLUTVIN, *J. Phis. Khim.* **30** (1956) 2251.
48. P. I. LOEFF, A. W. WEEBER and A. R. MIEDEMA, *J. Less-Common Metals* **140** (1988) 299.
49. P. I. LOEFF, H. BAKKER and F. R. de BOER, in "Proceedings of the DGM Conference on New Materials by Mechanical Alloying Techniques", edited by E. Arzt and L. Schultz (Deutsche Gesellschaft fur Metallkunde e.v., 1989) p. 119.

Received and accepted 12 January 1994